Optimal Level-Crossing Prediction for Jump Linear MIMO Dynamical Systems

Rodney A. Martin, *Member, IEEE*

***Abstract*—In this article, the theoretically optimal prediction of level-crossings for a jump linear MIMO (multi-input multi-output) dynamical system driven by operator input is investigated. The study of this problem is motivated by the practical implications for design of an optimal alarm system as applied to the advance prediction of fuel flow overages, which will elicit the fewest false alarms for a fixed detection probability. This work also introduces the use of a hidden Markov model (HMM) to allow for the modeling of operator input dynamics in tandem with the jump linear MIMO dynamical system that represents aircraft dynamics. It is shown that using an HMM to model operator input dynamics results in better prediction performance and qualitatively has a higher model fidelity than when using a jump linear MIMO dynamical system for the same function.**

***Index Terms*—Alarm systems, Hidden Markov models, Kalman filtering, Level-crossing problems, Prediction methods**

I. Introduction

An article recently published [1] introduced a novel approach of combining the practical appeal of Kalman filtering with the design of an optimal alarm system for the prediction of level-crossing events. However, practical application of this technique to the prediction of adverse events in aviation data required the use of a serial architecture to preprocess a full feature space, implicitly reducing it to a univariate signal while retaining salient dynamic characteristics [2]. This step was necessary due to existing technical constraints implicit in the use of the method as introduced in [1]. As such, data reduction was performed by using a regression algorithm to predict a target value relevant to safe operation based upon the full feature space. The resulting residual had properties which were favorable for use as training data to learn the parameters of a linear dynamical system.

In this paper these restrictions are lifted so as to allow for exposure to a broader class of models while also potentially helping to characterize mode-dependent nonlinearities that may be found in the data. Specifically, the basic technique is extended to allow for the use of a switched multi-input/multi-output (MIMO) linear dynamical system. Unlike jump linear dynamical systems or the switched Kalman filter whose dynamics switch according to the evolution of a Markov chain, switching will take place in a purely deterministic fashion. The determinism is governed by a potentially exponential number of modes as a consequence of the total number of available discrete inputs, which can be selected by an operator. The former type of jump linear dynamical system is well known and has been studied in previous work [3]-[4].

Even though the number of modes can potentially scale in an exponential fashion, the actual number of modes typically scale in a favorable manner due in part to natural operational and practical constraints. Thus, the proposed technique implicitly yet fundamentally extends previous variants to allow for the processing of multivariate heterogeneous (both discrete and continuous) data in lieu of just univariate continuous data. This also obviates the need for the use of a preprocessing regression algorithm in serial with the linear dynamical system having a univariate output as presented in [2]. However, all potential system nonlinearities must now be characterized purely upon mode changes rather than upon the underlying model itself due to the absence of a nonlinear regression algorithm that acts as a static nonlinear transformation of input data. In future work a static nonlinear mapping may be placed in series with the jump MIMO linear dynamical system, as was performed in [5]. The purpose of doing so will be to characterize the underlying system nonlinearities in addition to those governed by mode switches, rather than for use in generating a residual.

In this paper, forecasts of level-crossings associated with residuals generated by the divergence between future values for a specifically designated monitored target and the predicted model value are abandoned in favor of a much more intuitive and practically relevant detection paradigm. Ostensibly, the former method captures the ability to predict future excursions of how well the monitored process adheres to the model, so the success of the technique relies heavily on having substantially high model fidelity. However, the new paradigm involves predicting excursions of future values of the monitored process itself, outside of predetermined envelopes in multiple dimensions. As such, the event to be predicted is associated with actual monitored values rather than a residual associated with a single monitored value. Model fidelity is still quite important in using the new paradigm, nonetheless, but the characterization operates on a different layer of abstraction. Quite simply, the model representing the underlying governing dynamics of the human-machine system requires a high fidelity in contrast to the need for high fidelity modeling of the dynamics embedded in a residual.

However, due to the fact that human operator input is now part of the problem construction, it is also necessary to develop models to generate forecasts of these future inputs. This requires the development of a cascading, serial end-to-

Manuscript received December 31, 2010; revised . This work was supported in part by the Integrated Vehicle Health Management (IVHM) project, funded by the Aviation Safety Program of NASA's Aeronautics Research Mission Directorate.

R A. Martin is with the Intelligent Systems Division and the Intelligent Data Understanding Group, NASA Ames Research Center, Mail Stop 269-1, Bldg. N269, Rm. 260-17, P.O. Box 1, Moffett Field, CA 94035-0001 USA (phone: 650-604-1334; e-mail: rodney.martin@nasa.gov).

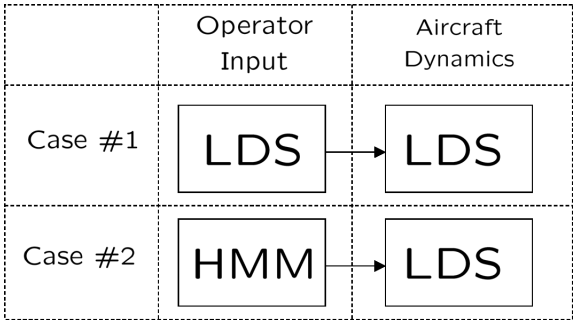

Fig. 1. Block diagrams two modeling representation for the human-machine system connected in a serial architecture

end collection of two models, the first characterizing human operator input, and the second one representing the aircraft dynamics as illustrated in Fig. 1. For this first model of human input, both a simple linear dynamical system and a standard Hidden Markov Model (HMM) will be investigated (shown as interchangeable blocks as Case #1 and Case #2 in Fig. 1) for the benefit of a contrasting performance assessment. The use of the HMM method to model human input is very similar to what was presented in previous work by Pavlovic *et al.* [6]. The performance of the overall system as quantified by the AUC (area under the ROC curve), and applied to the problem of fuel flow consumption initially studied by Srivastava [7] will be investigated, comparing both Cases #1 and #2.

II. Methodology

A multivariate level-crossing event is defined by the hyperbox $\times_{i=1}^{n_y}[\ell_i, \upsilon_i]$, where ℓ_i and υ_i are critical levels assumed to have a fixed, static values for each dimension. The primary objective of this paper is to predict when the trajectory of critical parameters represented by a vector-valued dynamic process, $\mathbf{y}_k \in \mathbb{R}^{n_y}$ leaves the hyperbox at some point in the future, for any dimension. This process will be modeled as a stationary multi-input multi-output (MIMO) jump linear dynamical system. The theory that follows is based upon this standard representation of the optimal level-crossing problem. The state-space formulation for the aircraft dynamics is shown in Eqns. 1-3, demonstrating propagation of both the state, $\mathbf{x}_k \in \mathbb{R}^{n_x}$ which is corrupted by process noise $\mathbf{w}_k \in \mathbb{R}^{n_x}$, and the state covariance matrix, $\mathbf{P}_k^x$, which evolve with the time-varying (mode dependent) system matrix $\mathbf{A}(\mathbf{z}_k)$.

Switching among model parameters such as the time-varying (mode dependent) system matrix is governed by $z_k \in \mathbb{Z}_m^+ \triangleq [1, \ldots m]$, where there are m observed operational modes. This switching is completely deterministic in nature, and governed by operation of all discrete inputs by the human operator. As such, the method described herein is fully capable of processing heterogeneous data. Note that the current representation for the operational mode, z_k, is as a discrete scalar value. A more formal vector-valued representation of the operational modes can be given by $\mathbf{z}_k \in \mathbb{B}^m \equiv \{0,1\}^m$, which may represent m binary switches in the cockpit of an aircraft, or if necessary $\mathbf{z}_k \in \mathbb{Z}_{n_l}^m \equiv \{0, \ldots, n_l - 1\}^m$, where n_l represents the number of discrete levels of the input variable. The more formal vector-valued representation for $\mathbf{z}_k$ will be used hereafter.

The output, $\mathbf{y}_k \in \mathbb{R}^{n_y}$ is multivariate, and is corrupted by measurement noise $\mathbf{v}_k \in \mathbb{R}^{n_y}$. The input, $\mathbf{u}_k \in \mathbb{R}^{n_u}$ is also multivariate, thus there are n_u inputs and n_y outputs for the jump linear MIMO dynamical system (LDS). The state space formulation for the human operator input is provided in Eqns. 4 - 6 when using a linear dynamical system (LDS) representation, and Eqns. 5, 7-10 when using an HMM (Hidden Markov Model) representation. In the latter case, for Eqn. 8 there are M possible hidden states of human operation such that $\mathbf{q}_k \in \mathbb{Z}_M^+$. Eqn. 5 can be used to represent the resulting input for either the HMM or the LDS. When human operation is modeled as an LDS, propagation of both the state and covariance matrix evolve in a similar manner to the equations that govern aircraft dynamics. In this case however, the state, $\mathbf{q}_k \in \mathbb{R}^{n_q}$ is corrupted by process noise $\eta_k \in \mathbb{R}^{n_q}$, and evolves with the time-varying system matrix $\mathbf{G}(\mathbf{z}_k)$, as does the state covariance matrix, $\mathbf{P}_k^q$. The output of this dynamical system, $\mathbf{u}_k \in \mathbb{R}^{n_u}$ is multivariate, and naturally also acts as the input to the equations governing the aircraft dynamics as illustrated in Fig. 1. Eqn. 5 provides the formula for modeling $\mathbf{u}_k \in \mathbb{R}^{n_u}$, which is also corrupted by measurement noise $\gamma_k \in \mathbb{R}^{n_u}$.

$$\mathbf{x}_{k+1} = \mathbf{A}(\mathbf{z}_k)\mathbf{x}_k + \mathbf{B}(\mathbf{z}_k)\mathbf{u}_k + \mathbf{w}_k \quad (1)$$
$$\mathbf{y}_k = \mathbf{C}(\mathbf{z}_k)\mathbf{x}_k + \mathbf{D}(\mathbf{z}_k)\mathbf{u}_k + \mathbf{v}_k \quad (2)$$
$$\mathbf{P}_{k+1}^x = \mathbf{A}(\mathbf{z}_k)\mathbf{P}_k^x\mathbf{A}^\top(\mathbf{z}_k) + \mathbf{Q}(\mathbf{z}_k) \quad (3)$$
$$\mathbf{q}_{k+1} = \mathbf{G}(\mathbf{z}_k)\mathbf{q}_k + \eta_k \quad (4)$$
$$\mathbf{u}_k = \mathbf{H}(\mathbf{z}_k)\mathbf{q}_k + \gamma_k \quad (5)$$
$$\mathbf{P}_{k+1}^q = \mathbf{G}(\mathbf{z}_k)\mathbf{P}_k^q\mathbf{G}^\top(\mathbf{z}_k) + \mathbf{Q}(\mathbf{z}_k) \quad (6)$$
$$p(\mathbf{q}_{k+1}|\mathbf{q}_k) = \mathbf{q}_{k+1}^\top\mathbf{G}(\mathbf{z}_k)\mathbf{q}_k \quad (7)$$
$$\pi_k \triangleq p(\mathbf{q}_k) \equiv \begin{bmatrix} p(q_k = 1) \\ \vdots \\ p(q_k = M) \end{bmatrix} \quad (8)$$
$$p(\mathbf{q}_0) = \pi_0 \quad (9)$$
$$\pi_{k+1} = \mathbf{G}^\top(\mathbf{z}_k)\pi_k \quad (10)$$

where

$$\begin{aligned} \mathbf{w}_k &\sim \mathcal{N}(\mathbf{0}, \mathbf{Q}(\mathbf{z}_k)), \quad \mathbf{Q}(\mathbf{z}_k) \succeq \mathbf{0} \\ \mathbf{v}_k &\sim \mathcal{N}(0, \mathbf{R}(\mathbf{z}_k)), \quad \mathbf{R}(\mathbf{z}_k) \succeq \mathbf{0} \\ \eta_k &\sim \mathcal{N}(\mathbf{0}, \mathbf{\Omega}(\mathbf{z}_k)), \quad \mathbf{\Omega}(\mathbf{z}_k) \succeq \mathbf{0} \\ \gamma_k &\sim \mathcal{N}(0, \mathbf{\Gamma}(\mathbf{z}_k)), \quad \mathbf{\Gamma}(\mathbf{z}_k) \succeq \mathbf{0} \\ \mathbf{x}_0 &\sim \mathcal{N}(\mu_{\mathbf{x}}(\mathbf{z}_0), \mathbf{P}_0^x(\mathbf{z}_0)) \\ \mathbf{q}_0 &\sim \mathcal{N}(\mu_{\mathbf{q}}(\mathbf{z}_0), \mathbf{P}_0^q(\mathbf{z}_0)) \end{aligned}$$

A summary of the basic mathematical notation not defined elsewhere is provided in Table I. There is great flexibility in constructing a mathematical representation for the level-crossing event, C_k. Ostensibly, the target application will drive the definition of this event. As such, in this paper the event of interest is shown in Eqn. 11, in consideration of the motivating factors described in [1]. This level-crossing event represents

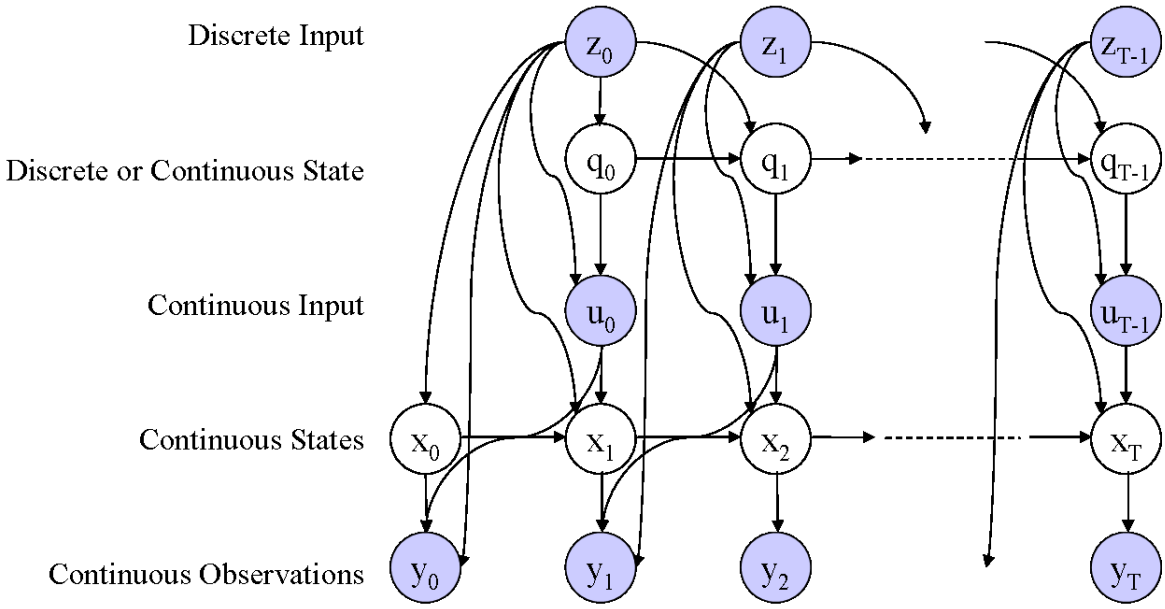

Fig. 2. Dynamic Bayesian Network

Mathematical Representation	*Nomenclature*
$\succeq$	Positive semi-definite
$(\bullet)'$	Not (Set complement)
$\mathcal{I}$	Universe of all events
$(\bullet)^\top$	Transpose
$P(\bullet)$	Probability
$E[\bullet]$ or $\mu_\bullet$	Expected Value
$\hat{\bullet}_{k+j\|k}$	$E[\bullet\|y_0,\ldots,y_k]$ (Conditional Expectation)
$\tilde{\bullet}_k$	Orthonormal rotation of $\bullet_k$ in vector space
$\bullet^*$	Result of vector space orthonormal rotation in probability or event space
$\mathcal{N}(\mu,\Sigma)$	Gaussian distribution with mean μ and covariance Σ
$\mathcal{N}(\mathbf{x};\mu,\Sigma)$	Gaussian distribution evaluated at $\mathbf{x}$ with mean μ and covariance Σ

TABLE I
SUMMARY OF MATHEMATICAL NOTATION

at least one exceedance outside of the hyperbox specified by $\mathcal{S}\triangleq\times_{i=1}^{n_y}[\ell_i,\upsilon_i]$ of the process $\mathbf{y}_k$ within the specified look-ahead prediction window, d.

$$C_k \triangleq \bigcup_{j=1}^{d} S_{k+j} = \bigcup_{j=1}^{d} E'_{k+j} = \mathcal{I}\setminus\bigcap_{j=1}^{d} E_{k+j} \quad (11)$$

where

$$E_{k+j} \triangleq \{\mathbf{y}_{k+j}\in\mathcal{S}\},\ \forall j\geq 1$$
$$S_{k+j} \triangleq \begin{cases} E'_{k+j} & j=1 \\ \bigcap_{i=1}^{j-1} E_{k+i}, E'_{k+j} & \forall j>1 \end{cases}$$

Developing algorithms for models that have a level of complexity characterized by Eqns. 1-10 above can often be complemented by a more intuitive expression with the aid of a probabilistic graphical model, or DBN (Dynamic Bayesian Network). This allows for the expression of topological invariance inherent in using either of the cases illustrated in Fig. 1. An illustration of the jump MIMO linear dynamical system representing either case is provided in Fig. 2.

The event C_k can be represented as the union of disjoint subevents, S_{k+j}, or as the union of overlapping subevents, E'_{k+j}. However, due to DeMorgan's theorem, the latter can be expressed in a more compact fashion via a *single* term when computing the probability of the overall event. This obviates the need for use of the inclusion/exclusion rule for the realization of all relevant terms in a probability computation based upon the union of overlapping subevents, E'_{k+j}, where the number of terms would be exponential in d. It also obviates the need for computing the probability based upon the former union of disjoint subevents, S_{k+j}, where there is no need for use of the inclusion/exclusion rule. However, the number of terms would still be linear in d, as the probability computation of the union of disjoint subevents is represented by the sum of terms involving S_{k+j}. Thus Eqn. 12 represents the unconditional probability of the level-crossing event in its most compact representational form.

$$P(C_k) = 1-\underbrace{\int_{-\ell_1}^{\upsilon_1}\cdots\int_{-\ell_{n_y}}^{\upsilon_{n_y}}\cdots}_{1}$$
$$\cdots\underbrace{\int_{-\ell_1}^{\upsilon_1}\cdots\int_{-\ell_{n_y}}^{\upsilon_{n_y}}}_{d}\mathcal{N}(\mathbf{y}_d;\mu_{\mathbf{y}_d},\Sigma_{\mathbf{y}_d})d\mathbf{y}_d \quad (12)$$

where

$$\mathbf{y}_d \triangleq \begin{bmatrix} \mathbf{y}_{k+1} \\ \vdots \\ \mathbf{y}_{k+d} \end{bmatrix}$$

Refer to Figs. 8 and 10 for Case #1 (the cascaded linear dynamical systems), and Fig. 11 for Case #2 (the HMM in series with the linear dynamical system), both located in Appendix A, for expressions of $\mu_{\mathbf{y}_d}$ and $\Sigma_{\mathbf{y}_d}$. $\Sigma_{\mathbf{y}_d}$ can also be approximated by substituting the steady-state versions of the Lyapunov equation given previously as Eqns. 3 and 6, $\mathbf{P}^L_{xx}$, in place of $\mathbf{P}^x_k$ and $\mathbf{P}^L_{qq}$, in place of $\mathbf{P}^q_k$, which agrees with the assumption of stationarity. Also, specific to Case #2, the stationary Markov distribution, π_{qq} is used in place of π_k, which is also the solution to Eqn. 10 when making the appropriate steady-state substitution. The solution, π_{qq}, is nothing more than the eigenvector corresponding to the eigenvalue $\lambda(\mathbf{G}^\top(\mathbf{z}_k)) = 1$. The approximations are shown in Figs. 8, 10 and 11 located in Appendix A. Note that $\mu_{\mathbf{y}_d}$ and $\Sigma_{\mathbf{y}_d}$ are still dependent upon $\mathbf{z}_k$, and ostensibly counter the argument of stationarity. However, the parameters associated with $\mathbf{z}_k$ are unique to each instance of the corresponding operational mode. As such, the assumption of "local" stationarity is valid for each operational mode as defined by $\mathbf{z}_k$.

These approximations, while introducing error with regards to the probability of a level-crossing event, $P(C_k)$ at a specific point in time, k, is negligible and will provide for a great computational advantage in the design of an alarm system. Instead of designing an alarm system for each time step, a single alarm system is designed for all time steps. The approximation is based upon the limiting statistics that are reached at steady-state, which greatly reduces the computational burden. An enabling theorem which can be found in [1] provides the mathematical underpinnings for the optimal alarm condition corresponding to the level-crossing event, shown here as Eqn. 13. Alternatively, the optimal alarm condition derived in [1] can be expressed in terms of the subevents E_{k+j}, as shown in Eqn. 14.

$$P(C_k|\mathbf{y}_0,\ldots,\mathbf{y}_k) \geq P_b \tag{13}$$

$$\Leftrightarrow P\left(\bigcap_{j=1}^{d} E_{k+j}|\mathbf{y}_0,\ldots,\mathbf{y}_k\right) \leq 1-P_b \tag{14}$$

The optimal alarm condition has therefore been derived from the use of the likelihood ratio resulting in the conditional inequality as given in Eqn. 13. This basically says "give alarm when the conditional probability of the event, C_k, exceeds the level P_b." Here, P_b represents some optimally chosen border or threshold probability with respect to a relevant alarm system metric. It is necessary to find the alarm regions in order to design the alarm system. This alarm region is parameterized by future process output predictions and covariances, for the aircraft dynamics, Case #1, and Case #2.

A. Optimal Alarm System

A more formal representation of the optimal alarm region is shown in Eqn. 46 of Fig. 6, which essentially defines a sublevel set of $g(\hat{\mathbf{y}}_d) \triangleq P\left(\bigcap_{j=1}^{d} E_{k+j}|\mathbf{y}_0,\ldots,\mathbf{y}_k\right)$ as a function of $\hat{\mathbf{y}}_d$. Eqn. 15 of Fig. 3 gives the multivariate normal probability computation to be performed via numerical integration, required for enabling the optimal alarm condition.

The feasible region for values of P_b can easily be determined by applying an intermediate value theorem from calculus which provides sufficient conditions for finding a level set solution. The sufficient conditions are shown as Eqns. 17-18, and the resulting level set shown as Eqn. 19 represents the locus of points that spans both the prediction horizon as well as the space spanned by $\mathbf{y}_k \in \mathbb{R}^{n_y}$.

$$g(\mu_{\mathbf{y}_d}) \geq 1-P_b \tag{17}$$

$$\lim_{|\hat{\mathbf{y}}_d|\setminus\hat{y}^i_{k+j|k}\to\infty} g(\hat{\mathbf{y}}_d) < 1-P_b, \quad \forall j \in [1,\ldots,d] \tag{18}$$

$$L_A \triangleq \left\{ \bigcap_{j=1}^{d}\bigcap_{i=1}^{n_y} \hat{y}^i_{k+j|k} : g(\hat{\mathbf{y}}_d) = 1-P_b \right\} \tag{19}$$

The notation that represents the limiting condition shown in Eqn. 18 is $|\hat{\mathbf{y}}_d|\setminus\hat{y}^i_{k+j|k} \to \infty$, and is meant to indicate that all elements of $\hat{\mathbf{y}}_d$ other than $\hat{y}^i_{k+j|k}$ approach $\pm\infty$. Application of this condition yields $P_b < 1$, which is true by definition, and application of the sufficient condition shown in Eqn. 17 yields $P_b \geq 1 - g(\mu_{\mathbf{y}_d})$. Thus the feasible region for P_b is $P_b \in [1-g(\mu_{\mathbf{y}_d}), 1]$.

It is not possible to obtain an exact closed-form representation of the parametrization for the optimal alarm region shown in Eqn. 46. As such, a Monte Carlo approach must be used to provide the best approximation of the exact alarm region, given sufficient samples. This allows the ROC curve statistics to be estimated empirically with observational truth data generated from the existing model and corresponding computations of the conditional probability of level-crossing events given by Eqn. 15.

B. Aircraft Dynamics

Process output predictions and covariances for the aircraft dynamics can be derived from standard Kalman filter Eqns. 20 - 25 as shown in Fig. 4. $\mathbf{P}^R_{xx}$ is the combined steady-state version of Eqns. 24 and 25, or the discrete algebraic Riccati equation, and $\hat{\mathbf{P}}^R_{xx}$ is the steady-state *a posteriori* covariance matrix given in Eqn. 31. Eqn. 32 is also used in Eqn. 31, which is the steady-state version of the Kalman gain from Eqn. 23.

The approximations shown in Eqns. 28 and 30 will provide for a great computational advantage in design of the optimal alarm system and its corresponding approximations for reasons stated previously. Due to the approximation of $\mathbf{P}^x_{k|k}$ with $\hat{\mathbf{P}}^R_{xx}$ shown in these equations, the Kalman filter will be suboptimal, as cited by Lewis [8]. However, the assumption of stationarity is required for the design of an optimal alarm system as defined by the respective enabling theorem cited in [1], and holds here as well.

C. Case #1 (LDS Model of Operator Input)

Process output predictions and covariances for Case #1 can be derived from standard Kalman filter Eqns. 33- 38 as shown

$$
\begin{aligned}
P\left(\bigcap_{j=1}^{d} E_{k+j}|\mathbf{y}_0,\ldots,\mathbf{y}_k\right) &= \underbrace{\int_{-\ell_1}^{\upsilon_1}\cdots\int_{-\ell_{n_y}}^{\upsilon_{n_y}}}_{1}\cdots\underbrace{\int_{-\ell_1}^{\upsilon_1}\cdots\int_{-\ell_{n_y}}^{\upsilon_{n_y}}}_{d}\mathcal{N}(\mathbf{y}_d;\hat{\mathbf{y}}_d,\hat{\Sigma}_{\mathbf{y}_d})d\mathbf{y}_d \qquad (15)\\
&= \underbrace{\int_{-\ell_1-\hat{y}^1_{k+1|k}}^{\upsilon_1-\hat{y}^1_{k+1|k}}\cdots\int_{-\ell_{n_y}-\hat{y}^{n_y}_{k+1|k}}^{\upsilon_{n_y}-\hat{y}^{n_y}_{k+1|k}}}_{1}\cdots\underbrace{\int_{-\ell_1-\hat{y}^1_{k+1|k}}^{\upsilon_1-\hat{y}^1_{k+1|k}}\cdots\int_{-\ell_{n_y}-\hat{y}^{n_y}_{k+1|k}}^{\upsilon_{n_y}-\hat{y}^{n_y}_{k+1|k}}}_{d}\mathcal{N}(\mathbf{y}_d;\mathbf{0}_d,\hat{\Sigma}_{\mathbf{y}_d})d\mathbf{y}_d\\
\hat{\mathbf{y}}_d &\triangleq E[\mathbf{y}_d|\mathbf{y}_0,\ldots,\mathbf{y}_k]=\begin{bmatrix}\hat{\mathbf{y}}_{k+1|k}\\ \vdots\\ \hat{\mathbf{y}}_{k+d|k}\end{bmatrix} \qquad (16)
\end{aligned}
$$

where $\hat{\mathbf{y}}_d$ is as defined in Eqn. 16, and $\hat{\Sigma}_{\mathbf{y}_d}$ for both Cases #1 and #2 can be found in App. A.

Fig. 3. Conditional Level-Crossing Probability

$$
\begin{aligned}
\hat{\mathbf{x}}_{k+1|k} &= \mathbf{A}(\mathbf{z}_k)\hat{\mathbf{x}}_{k|k}+\mathbf{B}(\mathbf{z}_k)\mathbf{u}_k && (20)\\
\hat{\mathbf{y}}_{k|k} &= \mathbf{C}(\mathbf{z}_k)\hat{\mathbf{x}}_{k|k}+\mathbf{D}(\mathbf{z}_k)\mathbf{u}_k && (21)\\
\hat{\mathbf{x}}_{k+1|k+1} &= \hat{\mathbf{x}}_{k+1|k}+\mathbf{F}^x_{k+1|k}\varepsilon^x_{k+1} && (22)\\
\mathbf{F}^x_{k+1|k} &\triangleq \mathbf{P}^x_{k+1|k}\mathbf{C}^\top(\mathbf{z}_k)\left[\mathbf{C}(\mathbf{z}_k)\mathbf{P}^x_{k+1|k}\mathbf{C}^\top(\mathbf{z}_k)+\mathbf{R}(\mathbf{z}_k)\right]^{-1} && (23)\\
\mathbf{P}^x_{k+1|k} &= \mathbf{A}(\mathbf{z}_k)\mathbf{P}^x_{k|k}\mathbf{A}^\top(\mathbf{z}_k)+\mathbf{Q}(\mathbf{z}_k) && (24)\\
\mathbf{P}^x_{k+1|k+1} &= \left(\mathbf{I}_{n_x}-\mathbf{F}^x_{k+1|k}\mathbf{C}(\mathbf{z}_k)\right)\mathbf{P}^x_{k+1|k} && (25)
\end{aligned}
$$

where

$$
\begin{aligned}
\hat{\mathbf{x}}_{k|k} &\triangleq E[\mathbf{x}_k|\mathbf{y}_0,\ldots,\mathbf{y}_k]\\
\mathbf{P}^x_{k|k} &\triangleq E[(\mathbf{x}_k-\hat{\mathbf{x}}_{k|k})(\mathbf{x}_k-\hat{\mathbf{x}}_{k|k})^\top|\mathbf{y}_0,\ldots,\mathbf{y}_k]\\
\varepsilon^x_k &\triangleq \mathbf{y}_k-\mathbf{C}(\mathbf{z}_k)\hat{\mathbf{x}}_{k|k-1}-\mathbf{D}(\mathbf{z}_k)\mathbf{u}_k
\end{aligned}
$$

Relevant predictions, covariances and cross-covariances are given below as Eqns. 26- 32, respectively.

$$
\begin{aligned}
\hat{\mathbf{y}}_{k+j|k} &= \mathbf{C}(\mathbf{z}_k)\mathbf{A}(\mathbf{z}_k)^j\hat{\mathbf{x}}_{k+j|k}+\mathbf{Z}_j\hat{\mathbf{q}}_{k|k} && (26)\\
\mathbf{P}^x_{k+j|k} &= \mathbf{A}(\mathbf{z}_k)^j(\mathbf{P}^x_{k|k}-\mathbf{P}^L_{xx})(\mathbf{A}^\top(\mathbf{z}_k))^j+\mathbf{P}^L_{xx} && (27)\\
&\approx \mathbf{A}(\mathbf{z}_k)^j(\hat{\mathbf{P}}^R_{xx}-\mathbf{P}^L_{xx})(\mathbf{A}^\top(\mathbf{z}_k))^j+\mathbf{P}^L_{xx} && (28)\\
\mathbf{P}^x_{k+i,k+j|k} &= \mathbf{A}(\mathbf{z}_k)^i(\mathbf{P}^x_{k|k}-\mathbf{P}^L_{xx})(\mathbf{A}^\top(\mathbf{z}_k))^j+\mathbf{P}^L_{xx}\left(\mathbf{A}^\top(\mathbf{z}_k)\right)^{j-i} && (29)\\
&\approx \mathbf{A}(\mathbf{z}_k)^i(\hat{\mathbf{P}}^R_{xx}-\mathbf{P}^L_{xx})(\mathbf{A}^\top(\mathbf{z}_k))^j+\mathbf{P}^L_{xx}\left(\mathbf{A}^\top(\mathbf{z}_k)\right)^{j-i} && (30)\\
\hat{\mathbf{P}}^R_{xx} &= \left(\mathbf{I}_{n_x}-\mathbf{F}_{xx}\mathbf{C}(\mathbf{z}_k)\right)\mathbf{P}^R_{xx} && (31)\\
\mathbf{F}_{xx} &= \mathbf{P}^R_{xx}\mathbf{C}^\top(\mathbf{z}_k)\left[\mathbf{C}(\mathbf{z}_k)\mathbf{P}^R_{xx}\mathbf{C}^\top(\mathbf{z}_k)+\mathbf{R}(\mathbf{z}_k)\right]^{-1} && (32)
\end{aligned}
$$

where $\mathbf{Z}_j$ and $\mathbf{P}^L_{xx}$ are as defined in Appendix A.

Fig. 4. Kalman Filter Formulae for Aircraft Dynamics

in Fig. 5. As before, $\mathbf{P}^R_{qq}$ is the combined steady-state version of Eqns. 37 and 38, and $\hat{\mathbf{P}}^R_{qq}$ is the steady-state *a posteriori* covariance matrix given in Eqn. 44. Eqn. 45 is used in Eqn. 44, which is the steady-state version of the Kalman gain from Eqn. 36. Again, using these steady-state substitutions introduces suboptimality and thus yields (negligible) error, however doing so allows for a reduction in alarm system design time.

For Case #1, ROC curve statistics can be generated by numerically integrating expressions for the computation of relevant multivariate normal probabilities with the aid of an approximation. As such, computationally intensive simulation runs using Monte-Carlo empirical estimation can be avoided. These multivariate probability computations are performed by using an adaptation of Genz's algorithm [9], which is based upon a robust and computationally efficient technique

$$\hat{\mathbf{q}}_{k+1|k} = \mathbf{G}(\mathbf{z}_k)\hat{\mathbf{q}}_{k|k} \tag{33}$$
$$\hat{\mathbf{u}}_{k|k} = \mathbf{H}(\mathbf{z}_k)\hat{\mathbf{q}}_{k|k} \tag{34}$$
$$\hat{\mathbf{q}}_{k+1|k+1} = \hat{\mathbf{q}}_{k+1|k} + \mathbf{F}^q_{k+1|k}\varepsilon^q_{k+1} \tag{35}$$
$$\mathbf{F}^q_{k+1|k} \triangleq \mathbf{P}^q_{k+1|k}\mathbf{H}^\top(\mathbf{z}_k)\left[\mathbf{H}(\mathbf{z}_k)\mathbf{P}^q_{k+1|k}\mathbf{H}^\top(\mathbf{z}_k) + \mathbf{\Gamma}(\mathbf{z}_k)\right]^{-1} \tag{36}$$
$$\mathbf{P}^q_{k+1|k} = \mathbf{G}(\mathbf{z}_k)\mathbf{P}^q_{k|k}\mathbf{G}^\top(\mathbf{z}_k) + \mathbf{\Omega}(\mathbf{z}_k) \tag{37}$$
$$\mathbf{P}^q_{k+1|k+1} = \left(\mathbf{I}_{n_q} - \mathbf{F}^q_{k+1|k}\mathbf{H}(\mathbf{z}_k)\right)\mathbf{P}^q_{k+1|k} \tag{38}$$

where

$$\hat{\mathbf{q}}_{k|k} \triangleq E[\mathbf{q}_k|\mathbf{u}_0,\ldots,\mathbf{u}_k]$$
$$\mathbf{P}^q_{k|k} \triangleq E[(\mathbf{q}_k - \hat{\mathbf{q}}_{k|k})(\mathbf{q}_k - \hat{\mathbf{q}}_{k|k})^\top|\mathbf{u}_0,\ldots,\mathbf{u}_k]$$
$$\varepsilon^q_k \triangleq \mathbf{u}_k - \mathbf{H}(\mathbf{z}_k)\hat{\mathbf{q}}_{k|k-1}$$

Relevant predictions, covariances and cross-covariances are given below as Eqns. 39- 45, respectively.

$$\hat{\mathbf{u}}_{k+j|k} = \mathbf{H}(\mathbf{z}_k)\mathbf{G}(\mathbf{z}_k)^j\hat{\mathbf{q}}_{k+j|k} \tag{39}$$
$$\mathbf{P}^q_{k+j|k} = \mathbf{G}(\mathbf{z}_k)^j(\mathbf{P}^q_{k|k} - \mathbf{P}^L_{qq})\left(\mathbf{G}^\top(\mathbf{z}_k)\right)^j + \mathbf{P}^L_{qq} \tag{40}$$
$$\approx \mathbf{G}(\mathbf{z}_k)^j(\hat{\mathbf{P}}^R_{qq} - \mathbf{P}^L_{qq})\left(\mathbf{G}^\top(\mathbf{z}_k)\right)^j + \mathbf{P}^L_{qq} \tag{41}$$
$$\mathbf{P}^q_{k+i,k+j|k} = \mathbf{G}(\mathbf{z}_k)^i(\mathbf{P}^q_{k|k} - \mathbf{P}^L_{qq})\left(\mathbf{G}^\top(\mathbf{z}_k)\right)^j + \mathbf{P}^L_{qq}\left(\mathbf{G}^\top(\mathbf{z}_k)\right)^{j-i} \tag{42}$$
$$\approx \mathbf{G}(\mathbf{z}_k)^i(\hat{\mathbf{P}}^R_{qq} - \mathbf{P}^L_{qq})\left(\mathbf{G}^\top(\mathbf{z}_k)\right)^j + \mathbf{P}^L_{qq}\left(\mathbf{G}^\top(\mathbf{z}_k)\right)^{j-i} \tag{43}$$
$$\hat{\mathbf{P}}^R_{qq} = \left(\mathbf{I}_{n_q} - \mathbf{F}_{qq}\mathbf{H}(\mathbf{z}_k)\right)\mathbf{P}^R_{qq} \tag{44}$$
$$\mathbf{F}_{qq} = \mathbf{P}^R_{qq}\mathbf{H}^\top(\mathbf{z}_k)\left[\mathbf{H}(\mathbf{z}_k)\mathbf{P}^R_{qq}\mathbf{H}^\top(\mathbf{z}_k) + \mathbf{\Gamma}(\mathbf{z}_k)\right]^{-1} \tag{45}$$

where $\mathbf{P}^L_{qq}$ is as defined in Appendix A.

Fig. 5. Kalman Filter Formulae for Case#1

designed to be used for integrations in multiple dimensions for multivariate normal distributions. This provides a tool necessary for the design of approximations to an optimal alarm system that was explored in previous work [1], in which the tradeoff between computational burden and accuracy for two approximations were compared. However, in this paper only the least computationally burdensome ("closed-form") approximation will be implemented. For detail on theoretical aspects regarding this approximation, the interested reader is directed to [1]. Implementation of the "closed-form" approximation translates here to the MIMO case without loss of generality.

However, the resulting implementation for the MIMO case will be reviewed briefly. The optimal alarm region, A_k, is approximated by an alarm region specified by $\bigcup_{j=1}^{d}\bigcup_{i=1}^{n_y} A_k^{i,j}$, with a successive approximation on $A_k^{i,j}$; $A_k^{i,j}$ is defined in Eqn. 49. Fundamentally, the approximation can be constructed by solving for asymptotic bounds on the exact alarm region.

$$A_k^{i,j} = \{\hat{y}^i_{k+j|k} : P\left(E^i_{k+j}|\mathbf{y}_0,\ldots,\mathbf{y}_k\right) \leq 1 - P_b\} \tag{49}$$

where

$$E^i_{k+j} \triangleq \ell_i \leq y^i_{k+j} \leq \upsilon_i$$

The successive approximation is required in order to obtain a closed-form representation and parametrization of the alarm region without having to resort to root-finding required for solving $P(E^i_{k+j}|\mathbf{y}_0,\ldots,\mathbf{y}_k) \leq 1 - P_b$, which is equivalent to $P(y^i_{k+j} \geq \upsilon_i|\mathbf{y}_0,\ldots,\mathbf{y}_k) + P(y^i_{k+j} \leq \ell_i|\mathbf{y}_0,\ldots,\mathbf{y}_k) \geq P_b$. This second approximation is given by Eqn. 47 shown in Fig. 6, which breaks this condition into the union of two constitutive inequalities. By using this successive approximation, the alarm region can now be represented in "closed-form," given by Eqn. 48 which is also shown in Fig. 6. $\Phi^{-1}(\cdot)$ represents the inverse cumulative normal standard distribution function, and $V^i_{k+j|k}$ is an element of $\mathbf{V}_{k+j|k}$ defined in App. A. Both $L_{i,j}$ and $U_{i,j}$ $\forall j \in [1,\ldots,d]$ and $\forall i \in [1,\ldots,n_y]$ represent the limits of integration for Eqns. 51-54 (not shown). These equations are valid for computing P_d and P_{fa} in order to construct an ROC curve using the "closed-form" approximation.

The domain of feasibility for this approximation now changes, and $P_{b_{crit}}$ takes on a new value, which differs from $P_{b_{crit}} = 1 - g(\mu_{\mathbf{y}_d})$ corresponding to the feasibility regions for the optimal alarm region. Using an argument similar to the one presented in [1], the "closed-form" approximation

$$A_k \triangleq \left\{ \bigcap_{j=1}^{d} \hat{\mathbf{y}}_{k+j|k} : P(C_k|\mathbf{y}_0,\ldots,\mathbf{y}_k) \geq P_b \right\} \tag{46}$$

$$\triangleq \left\{ \bigcap_{j=1}^{d} \bigcap_{i=1}^{n_y} \hat{y}^i_{k+j|k} : P(\bigcap_{j=1}^{d} E_{k+j}|\mathbf{y}_0,\ldots,\mathbf{y}_k) \leq 1-P_b \right\}$$

$$A_k^{i,j} \approx \left\{ \hat{y}^i_{k+j|k} : P(y^i_{k+j} \geq \upsilon_i|\mathbf{y}_0,\ldots,\mathbf{y}_k) \geq P_b \bigcup P(y^i_{k+j} \leq \ell_i|\mathbf{y}_0,\ldots,\mathbf{y}_k) \geq P_b \right\} \tag{47}$$

$$A_k \approx \bigcup_{j=1}^{d}\bigcup_{i=1}^{n_y} A_k^{i,j} \approx \bigcup_{j=1}^{d}\bigcup_{i=1}^{n_y} \underbrace{\ell_i - \sqrt{V^i_{k+j|k}}\Phi^{-1}(P_b)}_{L_{i,j}} \geq \hat{y}^i_{k+j|k} \geq \underbrace{\upsilon_i + \sqrt{V^i_{k+j|k}}\Phi^{-1}(P_b)}_{U_{i,j}} \tag{48}$$

Fig. 6. Alarm Condition

yields a value for $P_{b_{crit}}$ given in Eqn. 50. The alarm region and its approximation will have a similar appearance to the illustrations provided in [1], however the multidimensional alarm region will span both the parameter space and time, in lieu of just time (*i.e.* the prediction horizon).

$$P_{b_{crit}} = \max_i \Phi\left(\frac{\ell_i - \upsilon_i}{2\sqrt{V^i_{k+d|k}}}\right) \tag{50}$$

It is possible to generate formulae for the true and false positive rates as a function of $L_{i,j}$ and $U_{i,j}$ by appealing to Eqns. 51-52, where in place of A_k its approximation to $\bigcup_{j=1}^{d}\bigcup_{i=1}^{n_y} A_k^{i,j}$ may be used. The formula for $P(C_k)$ has already been introduced in Eqn. 12, and holds regardless of the alarm system approximation. Thus, only the additional expressions for $P(C_k, A_k)$ and $P(A_k)$ are necessary for computing P_d and P_{fa}. Formulae for supporting probabilities $P(A'_k)$ and $P(C'_k, A'_k)$ in Eqns. 53-54 are given in Fig. 9 of App. A (shown with the limits of integration).

True positive rate:

$$P_d = P(C_k|A_k) = \frac{P(C_k, A_k)}{P(A_k)} \tag{51}$$

False positive rate:

$$P_{fa} = P(A_k|C'_k) = \frac{P(C'_k, A_k)}{P(C'_k)} = \frac{P(A_k) - P(C_k, A_k)}{1 - P(C_k)} \tag{52}$$

$$P(A_k) \approx \begin{cases} P\left(\bigcup_{j=1}^{d}\bigcup_{i=1}^{n_y} A_k^{i,j}\right) & P_b > P_{b_{crit}} \\ 1 & P_b = P_{b_{crit}} \end{cases} \tag{53}$$

$$\approx \begin{cases} 1 - P\left(\bigcap_{j=1}^{d}\bigcap_{i=1}^{n_y} \left(A_k^{i,j}\right)'\right) & P_b > P_{b_{crit}} \\ 1 & P_b = P_{b_{crit}} \end{cases}$$

$$P(C_k, A_k) = \begin{cases} P(C_k) - P(A'_k) + P(C'_k, A'_k) & P_b > P_{b_{crit}} \\ P(C_k) & P_b = P_{b_{crit}} \end{cases} \tag{54}$$

D. Case #2 (HMM Model of Operator Input)

For Case #2, the Kalman filter predictor/corrector equations do not hold since an HMM is used for inferring the state $\mathbf{q}_k$. This distinction from Case #1 will have ramifications for alarm system design. As such, using the definitions provided in Eqns. 57-59 can be used for inference, which are governed by the evolution of the Markovian dynamics via Eqn. 60. The state estimate $\pi_{k|k}$ is easily found with the use of standard forward recursion formulae typically used for these purposes as found in [10]. Eqns. 55 and 56 provide the basic constructs.

$$\Lambda_{k+1} = \text{diag}(\Upsilon_{k+1})\mathbf{G}^\top(\mathbf{z}_k)\Lambda_k \tag{55}$$

$$\Lambda_0 = \text{diag}(\Upsilon_0)\pi_0 \tag{56}$$

$$\pi_{k|k} \triangleq E[\mathbf{q}_k|\mathbf{u}_0,\ldots,\mathbf{u}_k] = p(\mathbf{q}_k|\mathbf{u}_0,\ldots,\mathbf{u}_k) \tag{57}$$

$$\equiv \begin{bmatrix} p(q_k = 1|\mathbf{u}_0,\ldots,\mathbf{u}_k) \\ \vdots \\ p(q_k = M|\mathbf{u}_0,\ldots,\mathbf{u}_k) \end{bmatrix} \tag{58}$$

$$= \frac{\Lambda_k}{p(\mathbf{u}_0,\ldots,\mathbf{u}_k)} = \frac{\Lambda_k}{\sum_{i=1}^{M}\alpha(q_t = i)} \tag{59}$$

$$\pi_{k+1|k} = \mathbf{G}^\top(\mathbf{z}_k)\pi_{k|k} \tag{60}$$

where

$$\alpha(q_t = i) \triangleq p(\mathbf{u}_0,\ldots,\mathbf{u}_t, q_t = i)$$

$$\Lambda_k = \begin{bmatrix} \alpha(q_k = 1) \\ \vdots \\ \alpha(q_k = M) \end{bmatrix}$$

$$\Upsilon_k = \begin{bmatrix} p(\mathbf{u}_k|q_k = 1) \\ \vdots \\ p(\mathbf{u}_k|q_k = M) \end{bmatrix}$$

$$p(\mathbf{u}_k|q_k = i) = \mathcal{N}(\mathbf{u}_k; \mu_i(\mathbf{z}_k), \Gamma(\mathbf{z}_k))$$

$$\text{Note: } \mathbf{H}(\mathbf{z}_k) = \begin{bmatrix} \mu_1(\mathbf{z}_k) & \ldots & \mu_M(\mathbf{z}_k) \end{bmatrix}$$

The alarm system design ramifications that come as a result of the distinction between Cases #1 and #2 are tied to the fact that no closed-form or any other type of approximation is possible. This is due to the nature of the unique mathematical representation of the conditional mean and covariance when incorporating the HMM statistics. Furthermore, the covariance matrix $\hat{\Sigma}_{\mathbf{y}_d}$ provided in Fig. 11 of App. A is time varying. Thus, the benefit of making approximations of the type given by using $\mathbf{P}^L_{xx}$ in place of $\mathbf{P}^x_k$ are lost. As such, the conditional probability of a level-crossing event, $P(C_k|\mathbf{y}_0,\ldots,\mathbf{y}_k)$ must

be computed for each point in time, k, since a single alarm system cannot be designed for all time steps. Recall the fact that $\hat{\mathbf{y}}_d$ of Eqn. 16 and $\hat{\Sigma}_{\mathbf{y}_d}$ are dependent upon $\mathbf{z}_k$, but did not counter the argument of stationarity. The parameters associated with $\mathbf{z}_k$ were unique to each instance of the corresponding operational mode, hence allowing for "local" stationarity of the conditional distribution for each operational mode as defined by $\mathbf{z}_k$.

For Case #2, this issue has no bearing on our results; the claim of local stationarity cannot be made due to the fact that $\hat{\Sigma}_{\mathbf{y}_d}$ is time varying (provided in Fig. 11 of App. A). However, $\mathbf{P}_k^x$ is assumed to be stationary by using $\mathbf{P}_{xx}^L$ in its place, just as for Case #1. In Case #1, this assumption was used for the purposes of simplifying alarm system design. This unique assumption of stationary, however, is unnecessary for Case #2 since it will not reduce the computational burden. The conditional level-crossing probability needs to be computed at each time step anyway, and thus making the substitution only serves to introduce error and suboptimality, even though it is negligible. Nonetheless, this simplifying assumption will be used for the sake of consistency with Case #1.

The assumption of local stationarity *is* necessary however, when implicitly invoking the *unconditional* probability of a level-crossing event, $P(C_k)$. Note that there is no need for using Eqns. 51-54 to generate ROC curve statistics for Case #2 due to the fact that no closed-form or any other type of approximation is possible. Instead, the Monte Carlo method described previously is used to compute the conditional level-crossing probability for bootstrapping the construction of an ROC curve along with observational truth data generated by model simulation. However, use of this method implicates the use of the alarm condition defined by Eqn. 13, which tacitly assumes stationarity of the unconditional distribution governing the level-crossing event as proven in [1]. Otherwise, the more general form of the alarm condition shown as Eqn. 61 used to derive Eqn. 13 in [1] will be needed.

$$\frac{P(C_k^{'}|\mathbf{y}_0,\ldots,\mathbf{y}_k)P(C_k)}{P(C_k|\mathbf{y}_0,\ldots,\mathbf{y}_k)P(C_k^{'})} \leq \lambda \tag{61}$$

This more general form of the alarm condition is based upon the use of a non-stationary probability distribution of the level-crossing event $P(C_k)$. However, using this condition for alarm system design requires much more computational effort than when making the assumption of stationarity of the *unconditional* distribution of the level-crossing event, $P(C_k)$. As such, alarm system design must rely upon use of the stationary distribution, which is implicit in application of Eqn. 13.

III. Results & Discussion

The example to be used for presentation of the results has a specific application to the problem of fuel flow consumption for commercial aircraft, which was initially studied by Srivastava [7]. Both the average throttle position controlled by the pilot and corrected wind (the component of the relative wind aligned with the aircraft's heading) are used as predictors for the fuel flow on both engines of the twin engine aircraft. Mathematically, the average throttle position and corrected wind represent the inputs $\mathbf{u}_k$, and the fuel flow on both engines represent the outputs $\mathbf{y}_k$. The training data consists of 658 flights for 85 aircraft that have flown a specified city pair route, and the validation data consists of 129 flights for 9 aircraft that have flown 2 distinct city pairs, one which is the opposite route of the city pair used for training, another which is a city pair whose destination is the same as for the training data. There are 368 observed discrete operational modes, represented mathematically by $\mathbf{z}_k$, even though there are 17 discrete inputs. Thus only 368 of a possible $2^{17} = 131072$ are valid operational discrete binary switch configurations. It was unnecessary to model multi-level switches, since all discrete inputs were binary, thus $n_l = 2$.

Model training was broken into two distinct phases, based upon decoupling the DBN given in Fig. 2. The first phase of training is given by the top and bottom three layers that represents the continuous aircraft dynamics, excluding only the second layer of nodes from the top that represents the discrete or continuous state of the operator input dynamics. The second phase of training is given by the top three layers that represents the operator input dynamics, excluding the bottom two that represent the continuous aircraft dynamics. It is therefore evident that this phased training represents not only a topological decoupling but a functional decoupling as well. The EM algorithm [11]-[12] is used for both phases of training.

For Case #1 the LDS is used for both phases, where for Case #2 the LDS is is used only for the first phase, and the HMM is used for the second phase. As such, for both cases the first phase LDS model parameters are initialized with N4SID [13], with the state dimension selected by the same heuristic model order selection process introduced in previous work [2] and trained as a "supervised" input/output LDS (for all 368 operational modes). For Case #1, the second phase is trained as an "unsupervised" output only LDS using the same initialization and model order selection procedure, again for all 368 operational modes. For Case #2, the second phase is trained as an HMM, and initialized using K-means clustering, with the number of possible hidden states of human operation, M, determined by minimizing the Davies-Bouldin index [14] over a set of K-means clusterings. The Davies-Bouldin index provides a measure of appropriateness of data partitions by quantifying the similarity of clusters, and is calculated for each clustering up to a maximum number $M_{max} = \sqrt{T}$, where T is the data length. The means and covariances of the optimized number of clusters used for initialization purposes are held fixed throughout training, so that only the Markovian dynamics are updated during the training process.

Due to the fact that only the running sum of a finite block of training data needs to be stored in memory, training can be conducted in a highly scalable fashion. This is due to the nature of the parameter updates for the "M" step in the EM algorithm. The finite blocks of data are easily represented as a single flight, which can easily be loaded into memory incrementally. Otherwise, it would be impossible to load all 658 flights into memory for batch training. After a set of feasible models have been constructed out of the

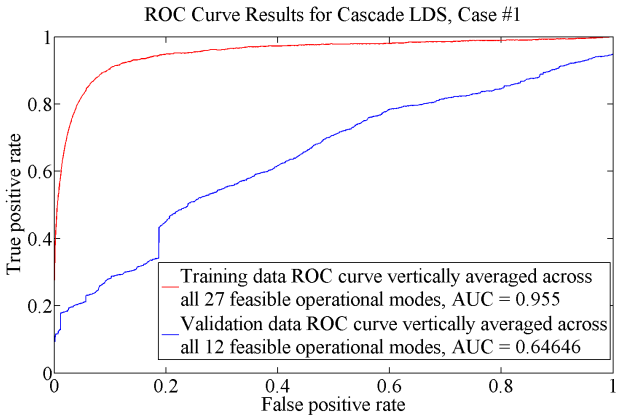

(a) Result for Case #1

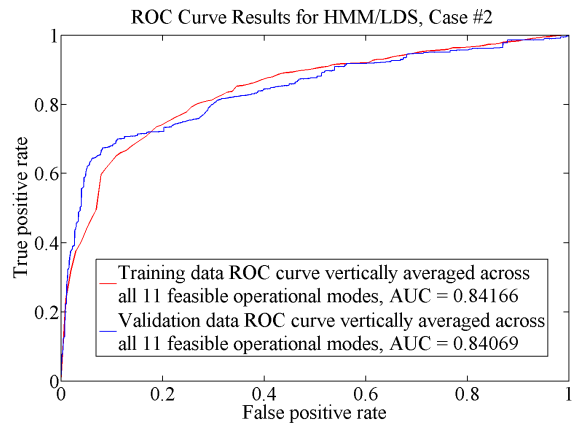

(b) Result for Case #2

Fig. 7. Results for Cases #1 & #2

possible 368 operational modes, alarm system design can take place. Reasons for model infeasibility of certain operational modes may range from having insufficient representation of data points available for model generation to the types of stability constraint problems as described in [2]. However, alarm system design and validation can be conducted for available feasible models according to the methods described in the previous section and in [2].

Briefly reviewing the details of validation ROC curve construction from [2], it is bootstrapped by computing the conditional level-crossing probability for each time point, based upon use of the appropriate model parameters and inference equations applied to real data. Additionally, the corresponding binary ground truth vector for each time point is obtained by advancing the vector forward by the number of indices corresponding a target 2 second prediction time horizon. Both of these vectors are necessary and sufficient for construction of an ROC curve. The design prediction time horizon used was $d = 5$ seconds. As in [2], the critical upper and lower threshold levels used for alarm system design can obtained by selecting an appropriate p-value associated with a reasonable confidence interval ($p = 0.05$) for the underlying Gaussian distribution made available by the modeling assumptions. However, in the multivariate case, the mapping from $p = 0.05$ to ℓ_i and υ_i, $\forall i \in [1, \ldots, n_y]$ is less mathematically straightforward than in the univariate case, and requires more sophisticated optimization methods to find the corresponding values. The overall alarm system results will be assessed by comparing the performance of the overall system as quantified by the AUC (area under the ROC curve) for both training and validation data, and for both Cases #1 and #2 in the following section.

IV. Conclusions & Future Work

The training and validation ROC curves averaged over a set of 27 and 12 feasible models corresponding to distinct operational modes for Case #1, respectively, are provided in Fig. 7(a). Similarly, training and validation ROC curves averaged over a set of 11 feasible models corresponding to distinct operational modes for Case #2 are provided in Fig. 7(b). As can easily be discerned, there is a large discrepancy between the reported training and validation AUC values for Case #1 as distinct from Case #2 where there is an almost negligible discrepancy between the reported training and validation AUC values. Furthermore, the more practically important result is that the validation AUC value for Case #1 is much higher than for Case #2.

As both Case #1 and #2 share the same modeling paradigm for aircraft dynamics, the previous observations speak to the improved ability of using an HMM to accurately characterize operator input dynamics over a simple LDS. In fact, it is clear that when using and LDS to model operator input dynamics the expected performance is overly optimistic as implied by the large discrepancy between the reported very high training AUC value and very low validation AUC value for Case #1. As such, the model fidelity may be low for this particular human-machine scenario when using cascading linear dynamical systems. A final conclusion that one may draw from these observations is that the model fidelity may be higher for Case #2 due to the improved ability of the HMM to characterize the human-machine scenario, and more specifically the operator input dynamics. The is due in part to the fact that the operator input dynamics are largely influenced by the initial K-means clustering optimization performed prior to the learning stage, where no such clustering is possible using a standard LDS.

As a concluding comment, it is noted that the results may in fact be heavily influenced by selection of free design parameters d, ℓ_i and υ_i, $\forall i \in [1, \ldots, n_y]$, as well as the heuristics chosen for model order selection. In the case of the cascaded linear dynamical systems, it was found previously [2] that the final results were highly sensitive to selection of the model order. Although the HMM model of operator input dynamics was also bootstrapped by a heuristic selection of the number of clusters, the relative sensitivities between Case #1 and #2 in regards to this issue is worth further consideration. Thus, in future work these effects will be more thoroughly investigated. Furthermore, some of the reasons for the model infeasibility of certain operational modes will be studied in earnest as well. Specifically, the stability constraint

problems described in [2] were likely a key contributor to the large number of infeasible models. As such, future work will also involve the enforcement of stability throughout the entire identification and learning process, as suggested in recent work by [15], [16]. Finally, as mentioned in the introduction, in future work a static nonlinear mapping may be placed in series with the jump MIMO linear dynamical system, as was performed in [5]. Again, the purpose of doing so will be to characterize the underlying system nonlinearities in addition to those governed by mode switches, rather than for use in generating a residual as was already studied in previous work [2].

V. Acknowledgements

The author would like to thank Dr. Santanu Das and Dr. Kamalika Das for reviewing this article.

Appendix A
Means and Covariances

References

[1] R. Martin, "A state-space approach to optimal level-crossing prediction for linear gaussian processes," *IEEE Transactions on Information Theory*, vol. 56, no. 10, pp. 5083 –5096, October 2010.

[2] R. Martin and S. Das, "Near real-time optimal prediction of adverse events in aviation data," in *Proceedings of the AIAA Infotech@Aerospace Conference*, Atlanta, Georgia, April 2010.

[3] K. Murphy, "Switching Kalman Filters," Department of Computer Science, University of California, Berkeley, Technical Report, 1998.

[4] V. Pavlovic, J. M. Rehg, T.-J. Cham, and K. P. Murphy, "A dynamic Bayesian network approach to figure tracking using learned dynamic models," in *The Proceedings of the Seventh IEEE International Conference on Computer Vision*, vol. 1, 1999, pp. 94–101.

[5] H. J. Palanthandalam-Madapusi, D. S. Bernstein, and A. J. Ridley, "Space weather forecasting: Identifying periodically switching block-structured models to predict magnetic-field fluctuations," *IEEE Control Systems Magazine*, pp. 109–123, October 2007.

[6] V. Pavlovic, B. Frey, and T. Huang, "Time-series classification using mixed-state dynamic bayesian networks," in *IEEE Computer Society Conference on Computer Vision and Pattern Recognition*, vol. 2, 1999, p. 615 Vol. 2.

[7] A. N. Srivastava, "Greener aviation with virtual sensors: A case study," *Data Mining and Knowledge Discovery (pending)*, Submitted 2010.

[8] F. Lewis, *Applied Optimal Control & Estimation: Digital Design & Implementation*. Prentice Hall, Inc., 1992.

[9] A. Genz, "Numerical computation of multivariate normal probabilities," *Journal of Computational and Graphical Statistics*, vol. 1, pp. 141–149, 1992.

[10] L. Rabiner, "A tutorial on HMM and selected applications in speech recognition," *Proceedings of the IEEE*, vol. 77, no. 2, pp. 257–286, February 1989.

[11] Z. Ghahramani and G. E. Hinton, "Parameter estimation for linear dynamical systems," Department of Computer Science, University of Toronto, Technical Report CRG-TR-96-2, 1996.

[12] V. V. Digalakis, J. R. Rohlicek, and M. Ostendorf, "ML estimation of a stochastic linear system with the EM algorithm and its application to speech recognition," *IEEE Transactions on Speech and Audio Processing*, vol. 1, no. 4, pp. 431–442, 1993.

[13] P. V. Overschee and B. D. Moor, *Subspace Identification for Linear Systems, Theory, Implementation, Applications*. Kluwer Academic Publishers, 1996.

[14] D. L. Davies and D. W. Bouldin, "A Cluster Separation Measure," *IEEE Transactions on Pattern Analysis and Machine Intelligence*, vol. PAMI-1, no. 2, pp. 224–227, April 1979. [Online]. Available: http://dx.doi.org/10.1109/TPAMI.1979.4766909

[15] S. Siddiqi, B. Boots, and G. Gordon, "A constraint generation approach to learning stable linear dynamical systems," in *Advances in Neural Information Processing Systems 20*, J. Platt, D. Koller, Y. Singer, and S. Roweis, Eds. Cambridge, MA: MIT Press, 2008, pp. 1329–1336.

[16] S. L. Lacy and D. S. Bernstein, "Subspace identification with guaranteed stability using constrained optimization," *IEEE Transactions on Automatic Control*, vol. 48, no. 7, pp. 1259 – 1263, July 2003.

Rodney A. Martin (M'02) received the B.S. degree in mechanical engineering from Carnegie-Mellon University, Pittsburgh, PA in 1992, the M.S. degree in mechanical engineering from the University of California, Berkeley in 2000, and the Ph.D. in mechanical engineering from the University of California, Berkeley in 2004.

He spent nearly 5 years on active duty as a Naval Officer in the U.S. Navy prior to entering graduate school, and has worked as a Computer Engineer at NASA Ames Research Center since completing his Ph.D. degree in 2004. His research interests span the areas of fault detection, estimation, prediction, control theory, and machine learning. Most recently he has worked on applying techniques from these research areas to projects at NASA that address aviation safety and space propulsion systems. Dr. Martin is currently also a member of AIAA.

$$
\begin{aligned}
\mu_{\mathbf{y}_d} &= \mathbf{O}(\mathbf{z}_k)\mathbf{A}(\mathbf{z}_k)\mu_{\mathbf{x}} + \mathbf{M}(\mathbf{z}_k)(\mathbf{1}_{d+1} \otimes \mu_{\mathbf{u}}) \\
\mu_{\mathbf{u}} &\triangleq E[\mathbf{u}_k] \\
\mu_{\mathbf{x}} &\triangleq E[\mathbf{x}_k] \\
\mathbf{1}_{d+1} &\triangleq \left.\begin{bmatrix} 1 \\ \vdots \\ 1 \end{bmatrix}\right\} d+1 \\
\mathbf{O}(\mathbf{z}_k) &\triangleq \begin{bmatrix} \mathbf{C}(\mathbf{z}_k) \\ \vdots \\ \mathbf{C}(\mathbf{z}_k)\mathbf{A}(\mathbf{z}_k)^{d-1} \end{bmatrix} \\
\mathbf{M}(\mathbf{z}_k) &\triangleq \begin{bmatrix}
\mathbf{0}_{n_y \times n_u} & \mathbf{0}_{n_y \times n_u} & \cdots & \mathbf{0}_{n_y \times n_u} & \mathbf{D}(\mathbf{z}_k) & \mathbf{C}(\mathbf{z}_k)\mathbf{B}(\mathbf{z}_k) \\
\vdots & \vdots & & \mathbf{D}(\mathbf{z}_k) & \mathbf{C}(\mathbf{z}_k)\mathbf{B}(\mathbf{z}_k) & \mathbf{C}(\mathbf{z}_k)\mathbf{A}(\mathbf{z}_k)\mathbf{B}(\mathbf{z}_k) \\
\mathbf{0}_{n_y \times n_u} & \mathbf{0}_{n_y \times n_u} & & & \mathbf{C}(\mathbf{z}_k)\mathbf{A}(\mathbf{z}_k)\mathbf{B}(\mathbf{z}_k) & \vdots \\
\mathbf{0}_{n_y \times n_u} & \mathbf{D}(\mathbf{z}_k) & \mathbf{C}(\mathbf{z}_k)\mathbf{B}(\mathbf{z}_k) & \iddots & \vdots & \vdots \\
\mathbf{D}(\mathbf{z}_k) & \mathbf{C}(\mathbf{z}_k)\mathbf{B}(\mathbf{z}_k) & \mathbf{C}(\mathbf{z}_k)\mathbf{A}(\mathbf{z}_k)\mathbf{B}(\mathbf{z}_k) & \cdots & \cdots & \mathbf{C}(\mathbf{z}_k)\mathbf{A}(\mathbf{z}_k)^{d-1}\mathbf{B}(\mathbf{z}_k)
\end{bmatrix}
\end{aligned}
$$

Fig. 8. Formulae for $\mu_{\mathbf{y}_d}$, Case #1

$$
\begin{aligned}
P(A'_k) \approx P\left(\bigcap_{j=1}^{d}\bigcap_{i=1}^{n_y}\left(A_k^{i,j}\right)'\right) &= P\left(\bigcap_{j=1}^{d}\bigcap_{i=1}^{n_y} L_{i,j} \le \hat{y}^i_{k+j|k} \le U_{i,j}\right) \\
&\approx \underbrace{\int_{L_{1,1}}^{U_{1,1}} \cdots \int_{L_{n_y,1}}^{U_{n_y,1}}}_{1} \cdots \underbrace{\int_{L_{1,d}}^{U_{1,d}} \cdots \int_{L_{n_y,d}}^{U_{n_y,d}}}_{d} \mathcal{N}(\hat{\mathbf{y}}_d; \mu_{\mathbf{y}_d}, \hat{\Sigma}_{\hat{\mathbf{y}}_d}) d\mathbf{y}_d
\end{aligned}
$$

and

$$
\hat{\Sigma}_{\hat{\mathbf{y}}_d} \triangleq \Sigma_{\mathbf{y}_d} - \hat{\Sigma}_{\mathbf{y}_d}
$$

For Case #1 (only) the expression for $\hat{\Sigma}_{\hat{\mathbf{y}}_d}$ simplifies to

$$
\hat{\Sigma}_{\hat{\mathbf{y}}_d} = \mathbf{O}(\mathbf{z}_k)(\mathbf{P}^L_{ss} - \mathbf{P}^R_{ss})\mathbf{O}^\top(\mathbf{z}_k) + \begin{bmatrix} \mathbf{Z}_1 \\ \vdots \\ \mathbf{Z}_d \end{bmatrix} (\mathbf{P}^L_{qq} - \hat{\mathbf{P}}^R_{qq}) \begin{bmatrix} \mathbf{Z}_1 \\ \vdots \\ \mathbf{Z}_d \end{bmatrix}^\top
$$

Note that $\mathbf{O}(\mathbf{z}_k)$ is defined in Fig. 8. Furthermore,

$$
\begin{aligned}
P(C'_k, A'_k) &\approx P\left(\bigcap_{j=1}^{d} E_{k+j}, \bigcap_{j=1}^{d}\bigcap_{i=1}^{n_y}\left(A_k^{i,j}\right)'\right) \\
&\approx \underbrace{\int_{-\ell_1}^{\upsilon_1} \cdots \int_{-\ell_{n_y}}^{\upsilon_{n_y}}}_{1} \cdots \underbrace{\int_{-\ell_1}^{\upsilon_1} \cdots \int_{-\ell_{n_y}}^{\upsilon_{n_y}}}_{d} \underbrace{\int_{L_{1,1}}^{U_{1,1}} \cdots \int_{L_{n_y,1}}^{U_{n_y,1}}}_{1} \cdots \underbrace{\int_{L_{1,d}}^{U_{1,d}} \cdots \int_{L_{n_y,d}}^{U_{n_y,d}}}_{d} \mathcal{N}(\mathbf{z}; \mu_{\mathbf{z}}, \Sigma_{\mathbf{z}}) d\mathbf{z}
\end{aligned}
$$

where

$$
\begin{aligned}
\mathbf{z} &\triangleq \begin{bmatrix} \mathbf{y}_d \\ \hat{\mathbf{y}}_d \end{bmatrix} \\
\mu_{\mathbf{z}} &\triangleq \begin{bmatrix} \mu_{\mathbf{y}_d} \\ \mu_{\mathbf{y}_d} \end{bmatrix} \\
\Sigma_{\mathbf{z}} &\triangleq \begin{bmatrix} \Sigma_{\mathbf{y}_d} & \hat{\Sigma}_{\hat{\mathbf{y}}_d} \\ \hat{\Sigma}_{\hat{\mathbf{y}}_d} & \hat{\Sigma}_{\hat{\mathbf{y}}_d} \end{bmatrix}
\end{aligned}
$$

Fig. 9. Relevant Alarm Statistics

$$
\begin{aligned}
\Sigma_{\mathbf{y}_d} &\triangleq \begin{cases} \mathbf{V}_{k+i} & \forall i = j \in [1,\ldots,d] \\ \mathbf{V}_{k+i,k+j} & \forall j > i \in [1,\ldots,d] \\ \mathbf{V}^\top_{k+i,k+j} & \forall j < i \in [1,\ldots,d] \end{cases} \\
\hat{\Sigma}_{\mathbf{y}_d} &\approx \begin{cases} \mathbf{V}_{k+i|k} & \forall i = j \in [1,\ldots,d] \\ \mathbf{V}_{k+i,k+j|k} & \forall j > i \in [1,\ldots,d] \\ \mathbf{V}^\top_{k+i,k+j|k} & \forall j < i \in [1,\ldots,d] \end{cases} \\
\mathbf{V}_{k+i} &\triangleq \mathbf{C}(\mathbf{z}_k)\mathbf{P}^x_k\mathbf{C}^\top(\mathbf{z}_k) + \mathbf{R}(\mathbf{z}_k) + \mathbf{Z}_i\mathbf{P}^q_k\mathbf{Z}^\top_i + \sum_{l=0}^{i-1}\mathbf{Z}_l\mathbf{\Omega}(\mathbf{z}_k)\mathbf{Z}^\top_l + \mathbf{D}(\mathbf{z}_k)\mathbf{\Gamma}(\mathbf{z}_k)\mathbf{D}^\top(\mathbf{z}_k) \\
&+ \mathbf{C}(\mathbf{z}_k)\left(\mathbf{P}^L_{qu} - \mathbf{A}^i(\mathbf{z}_k)\mathbf{P}^L_{qu}\left(\mathbf{A}^\top(\mathbf{z}_k)\right)^i\right)\mathbf{C}^\top(\mathbf{z}_k) \\
&\approx \mathbf{C}(\mathbf{z}_k)\mathbf{P}^L_{xx}\mathbf{C}^\top(\mathbf{z}_k) + \mathbf{R}(\mathbf{z}_k) + \mathbf{Z}_i\mathbf{P}^L_{qq}\mathbf{Z}^\top_i + \sum_{l=0}^{i-1}\mathbf{Z}_l\mathbf{\Omega}(\mathbf{z}_k)\mathbf{Z}^\top_l + \mathbf{D}(\mathbf{z}_k)\mathbf{\Gamma}(\mathbf{z}_k)\mathbf{D}^\top(\mathbf{z}_k) \\
&+ \mathbf{C}(\mathbf{z}_k)\left(\mathbf{P}^L_{qu} - \mathbf{A}^i(\mathbf{z}_k)\mathbf{P}^L_{qu}\left(\mathbf{A}^\top(\mathbf{z}_k)\right)^i\right)\mathbf{C}^\top(\mathbf{z}_k) \\
\mathbf{V}_{k+i,k+j} &\triangleq \mathbf{C}(\mathbf{z}_k)\left[\mathbf{A}^i(\mathbf{z}_k)(\mathbf{P}^x_k - \mathbf{P}^L_{xx})\left(\mathbf{A}^\top(\mathbf{z}_k)\right)^i\mathbf{P}^L_{xx}\left(\mathbf{A}^\top(\mathbf{z}_k)\right)^{j-i}\right]\mathbf{C}^\top(\mathbf{z}_k) + \mathbf{Z}_i\mathbf{P}^q_k\mathbf{Z}^\top_j + \sum_{l=0}^{i-1}\mathbf{Z}_l\mathbf{\Omega}(\mathbf{z}_k)\mathbf{Z}^\top_{l+j-i} \\
&+ \mathbf{C}(\mathbf{z}_k)\left(\mathbf{P}^L_{qu} - \mathbf{A}^i(\mathbf{z}_k)\mathbf{P}^L_{qu}\left(\mathbf{A}^\top(\mathbf{z}_k)^i\right)\right)\left(\mathbf{A}^\top(\mathbf{z}_k)\right)^{j-i}\mathbf{C}^\top(\mathbf{z}_k) \\
&\approx \mathbf{C}(\mathbf{z}_k)\mathbf{P}^L_{xx}\left(\mathbf{A}^\top(\mathbf{z}_k)\right)^{j-i}\mathbf{C}^\top(\mathbf{z}_k) + \mathbf{Z}_i\mathbf{P}^k_{qq}\mathbf{Z}^\top_j + \sum_{l=0}^{i-1}\mathbf{Z}_l\mathbf{\Omega}(\mathbf{z}_k)\mathbf{Z}^\top_{l+j-i} \\
&+ \mathbf{C}(\mathbf{z}_k)\left(\mathbf{P}^L_{qu} - \mathbf{A}^i(\mathbf{z}_k)\mathbf{P}^L_{qu}\left(\mathbf{A}^\top(\mathbf{z}_k)\right)^i\right)\left(\mathbf{A}^\top(\mathbf{z}_k)\right)^{j-i}\mathbf{C}^\top(\mathbf{z}_k) \\
\mathbf{V}_{k+i|k} &\triangleq \mathbf{C}(\mathbf{z}_k)\mathbf{P}^x_{k+i|k}\mathbf{C}^\top(\mathbf{z}_k) + \mathbf{R}(\mathbf{z}_k) + \mathbf{Z}_i\mathbf{P}^q_{k|k}\mathbf{Z}^\top_i + \sum_{l=0}^{i-1}\mathbf{Z}_l\mathbf{\Omega}(\mathbf{z}_k)\mathbf{Z}^\top_l + \mathbf{D}(\mathbf{z}_k)\mathbf{\Gamma}(\mathbf{z}_k)\mathbf{D}^\top(\mathbf{z}_k) \\
&+ \mathbf{C}(\mathbf{z}_k)\left(\mathbf{P}^L_{qu} - \mathbf{A}^i(\mathbf{z}_k)\mathbf{P}^L_{qu}\left(\mathbf{A}^\top(\mathbf{z}_k)\right)^i\right)\mathbf{C}^\top(\mathbf{z}_k) \\
&\approx \mathbf{C}(\mathbf{z}_k)\mathbf{P}^x_{k+i|k}\mathbf{C}^\top(\mathbf{z}_k) + \mathbf{R}(\mathbf{z}_k) + \mathbf{Z}_i\hat{\mathbf{P}}^R_{qq}\mathbf{Z}^\top_i + \sum_{l=0}^{i-1}\mathbf{Z}_l\mathbf{\Omega}(\mathbf{z}_k)\mathbf{Z}^\top_l + \mathbf{D}(\mathbf{z}_k)\mathbf{\Gamma}(\mathbf{z}_k)\mathbf{D}^\top(\mathbf{z}_k) \\
&+ \mathbf{C}(\mathbf{z}_k)\left(\mathbf{P}^L_{qu} - \mathbf{A}^i(\mathbf{z}_k)\mathbf{P}^L_{qu}\left(\mathbf{A}^\top(\mathbf{z}_k)\right)^i\right)\mathbf{C}^\top(\mathbf{z}_k) \\
\mathbf{V}_{k+i,k+j|k} &\triangleq \mathbf{C}(\mathbf{z}_k)\mathbf{P}^x_{k+i,k+j|k}\mathbf{C}^\top(\mathbf{z}_k) + \mathbf{Z}_i\mathbf{P}^q_{k|k}\mathbf{Z}^\top_j + \sum_{l=0}^{i-1}\mathbf{Z}_l\mathbf{\Omega}(\mathbf{z}_k)\mathbf{Z}^\top_{l+j-i} \\
&+ \mathbf{C}(\mathbf{z}_k)\left(\mathbf{P}^L_{qu} - \mathbf{A}^i(\mathbf{z}_k)\mathbf{P}^L_{qu}\left(\mathbf{A}^\top(\mathbf{z}_k)\right)^i\right)\left(\mathbf{A}^\top(\mathbf{z}_k)\right)^{j-i}\mathbf{C}^\top(\mathbf{z}_k) \\
&\approx \mathbf{C}(\mathbf{z}_k)\mathbf{P}^x_{k+i,k+j|k}\mathbf{C}^\top(\mathbf{z}_k) + \mathbf{Z}_i\hat{\mathbf{P}}^R_{qq}\mathbf{Z}^\top_j + \sum_{l=0}^{i-1}\mathbf{Z}_l\mathbf{\Omega}(\mathbf{z}_k)\mathbf{Z}^\top_{l+j-i} \\
&+ \mathbf{C}(\mathbf{z}_k)\left(\mathbf{P}^L_{qu} - \mathbf{A}^i(\mathbf{z}_k)\mathbf{P}^L_{qu}\left(\mathbf{A}^\top(\mathbf{z}_k)\right)^i\right)\left(\mathbf{A}^\top(\mathbf{z}_k)\right)^{j-i}\mathbf{C}^\top(\mathbf{z}_k) \\
\mathbf{P}^x_{k+i|k} &\approx \mathbf{A}(\mathbf{z}_k)^j(\hat{\mathbf{P}}^R_{xx} - \mathbf{P}^L_{xx})\left(\mathbf{A}^\top(\mathbf{z}_k)\right)^j + \mathbf{P}^L_{xx} \text{ (Recall Eqn.28)} \\
\mathbf{P}^x_{k+i,k+j|k} &\approx \mathbf{A}(\mathbf{z}_k)^i(\hat{\mathbf{P}}^R_{xx} - \mathbf{P}^L_{xx})\left(\mathbf{A}^\top(\mathbf{z}_k)\right)^j + \mathbf{P}^L_{xx}\left(\mathbf{A}^\top(\mathbf{z}_k)\right)^{j-i} \text{ (Recall Eqn.30)} \\
\text{where } \mathbf{Z}_{i+1} &= \mathbf{Z}_i\mathbf{G}(\mathbf{z}_k) + \mathbf{C}(\mathbf{z}_k)\mathbf{A}^i(\mathbf{z}_k)\mathbf{B}(\mathbf{z}_k)\mathbf{H}(\mathbf{z}_k), \quad \mathbf{Z}_0 = \mathbf{D}(\mathbf{z}_k)\mathbf{H}(\mathbf{z}_k) \\
\text{and } \mathbf{P}^L_{qu} &\triangleq \mathbf{B}(\mathbf{z}_k)\mathbf{\Gamma}(\mathbf{z}_k)\mathbf{B}^\top(\mathbf{z}_k) + \mathbf{A}(\mathbf{z}_k)\mathbf{P}^L_{qu}\mathbf{A}^\top(\mathbf{z}_k) \\
\mathbf{P}^L_{xx} &\triangleq \mathbf{A}(\mathbf{z}_k)\mathbf{P}^L_{xx}\mathbf{A}^\top(\mathbf{z}_k) + \mathbf{Q}(\mathbf{z}_k) \\
\mathbf{P}^L_{qq} &\triangleq \mathbf{G}(\mathbf{z}_k)\mathbf{P}^L_{qq}\mathbf{G}^\top(\mathbf{z}_k) + \mathbf{\Omega}(\mathbf{z}_k)
\end{aligned}
$$

Fig. 10. Formulae for $\Sigma_{\mathbf{y}_d}$ and $\hat{\Sigma}_{\mathbf{y}_d}$, Case #1

$$
\begin{aligned}
\mu_{\mathbf{y}_d} &= \mathbf{O}(\mathbf{z}_k)\mathbf{A}(\mathbf{z}_k)\mu_{\mathbf{x}} + \mathbf{M}(\mathbf{z}_k)\begin{bmatrix} \mathbf{H}(\mathbf{z}_k)\left(\mathbf{G}^\top(\mathbf{z}_k)\right)^d \\ \mathbf{H}(\mathbf{z}_k)\left(\mathbf{G}^\top(\mathbf{z}_k)\right)^{d-1} \\ \vdots \\ \mathbf{H}(\mathbf{z}_k)\mathbf{G}^\top(\mathbf{z}_k) \\ \mathbf{H}(\mathbf{z}_k) \end{bmatrix}\pi_k = \mathbf{O}(\mathbf{z}_k)\mathbf{A}(\mathbf{z}_k)\mu_{\mathbf{x}} + \begin{bmatrix} \mathbf{Z}_1 \\ \vdots \\ \mathbf{Z}_d \end{bmatrix}\pi_k \\
\Sigma_{\mathbf{y}_d} &\triangleq \begin{cases} \mathbf{V}_{k+i} & \forall i = j \in [1,\ldots,d] \\ \mathbf{V}_{k+i,k+j} & \forall j > i \in [1,\ldots,d] \\ \mathbf{V}^\top_{k+i,k+j} & \forall j < i \in [1,\ldots,d] \end{cases} \\
\hat{\Sigma}_{\mathbf{y}_d} &\approx \begin{cases} \mathbf{V}_{k+i|k} & \forall i = j \in [1,\ldots,d] \\ \mathbf{V}_{k+i,k+j|k} & \forall j > i \in [1,\ldots,d] \\ \mathbf{V}^\top_{k+i,k+j|k} & \forall j < i \in [1,\ldots,d] \end{cases} \\
\mathbf{V}_{k+i} &\triangleq \mathbf{C}(\mathbf{z}_k)\mathbf{P}^x_k\mathbf{C}^\top(\mathbf{z}_k) + \mathbf{R}(\mathbf{z}_k) + \mathbf{L}_i\left[\mathbf{I}_{i+1}\otimes\left(\mathrm{diag}(\pi_k) - \pi_k\pi_k^\top\right)\right]\mathbf{L}_i^\top + \mathbf{D}(\mathbf{z}_k)\mathbf{\Gamma}(\mathbf{z}_k)\mathbf{D}^\top(\mathbf{z}_k) \\
&+ \mathbf{C}(\mathbf{z}_k)\left(\mathbf{P}^L_{qu} - \mathbf{A}^i(\mathbf{z}_k)\mathbf{P}^L_{qu}\left(\mathbf{A}^\top(\mathbf{z}_k)\right)^i\right)\mathbf{C}^\top(\mathbf{z}_k) \\
&\approx \mathbf{C}(\mathbf{z}_k)\mathbf{P}^L_{xx}\mathbf{C}^\top(\mathbf{z}_k) + \mathbf{R}(\mathbf{z}_k) + \mathbf{L}_i\left[\mathbf{I}_{i+1}\otimes\left(\mathrm{diag}(\pi_{qq}) - \pi_{qq}\pi_{qq}^\top\right)\right]\mathbf{L}_i^\top + \mathbf{D}(\mathbf{z}_k)\mathbf{\Gamma}(\mathbf{z}_k)\mathbf{D}^\top(\mathbf{z}_k) \\
&+ \mathbf{C}(\mathbf{z}_k)\left(\mathbf{P}^L_{qu} - \mathbf{A}^i(\mathbf{z}_k)\mathbf{P}^L_{qu}\left(\mathbf{A}^\top(\mathbf{z}_k)\right)^i\right)\mathbf{C}^\top(\mathbf{z}_k) \\
\mathbf{V}_{k+i,k+j} &\triangleq \mathbf{C}(\mathbf{z}_k)\left[\mathbf{A}^i(\mathbf{z}_k)(\mathbf{P}^x_k - \mathbf{P}^L_{xx})\left(\mathbf{A}^\top(\mathbf{z}_k)\right)^i + \mathbf{P}^L_{xx}\left(\mathbf{A}^\top(\mathbf{z}_k)\right)^{j-i}\right]\mathbf{C}^\top(\mathbf{z}_k) \\
&+ \mathbf{L}_i\left[\mathbf{1}_{i+1}\mathbf{1}^\top_{j+1}\otimes\left(\mathrm{diag}(\pi_k) - \pi_k\pi_k^\top\right)\right]\mathbf{L}_j^\top + \mathbf{D}(\mathbf{z}_k)\mathbf{\Gamma}(\mathbf{z}_k)\mathbf{B}^\top(\mathbf{z}_k)\left(\mathbf{A}^\top(\mathbf{z}_k)\right)^{j-i-1}\mathbf{C}^\top(\mathbf{z}_k) \\
&+ \mathbf{C}(\mathbf{z}_k)\left(\mathbf{P}^L_{qu} - \mathbf{A}^i(\mathbf{z}_k)\mathbf{P}^L_{qu}\left(\mathbf{A}^\top(\mathbf{z}_k)\right)^i\right)\left(\mathbf{A}^\top(\mathbf{z}_k)\right)^{j-i}\mathbf{C}^\top(\mathbf{z}_k) \\
&\approx \mathbf{C}(\mathbf{z}_k)\mathbf{P}^L_{xx}\left(\mathbf{A}^\top(\mathbf{z}_k)\right)^{j-i}\mathbf{C}^\top(\mathbf{z}_k) + \mathbf{C}(\mathbf{z}_k)\left(\mathbf{P}^L_{qu} - \mathbf{A}^i(\mathbf{z}_k)\mathbf{P}^L_{qu}\left(\mathbf{A}^\top(\mathbf{z}_k)\right)^i\right)\left(\mathbf{A}^\top(\mathbf{z}_k)\right)^{j-i}\mathbf{C}^\top(\mathbf{z}_k) \\
&+ \mathbf{D}(\mathbf{z}_k)\mathbf{\Gamma}(\mathbf{z}_k)\mathbf{B}^\top(\mathbf{z}_k)\left(\mathbf{A}^\top(\mathbf{z}_k)\right)^{j-i-1}\mathbf{C}^\top(\mathbf{z}_k) + \mathbf{L}_i\left[\mathbf{1}_{i+1}\mathbf{1}^\top_{j+1}\otimes\left(\mathrm{diag}(\pi_{qq}) - \pi_{qq}\pi_{qq}^\top\right)\right]\mathbf{L}_j^\top \\
\mathbf{V}_{k+i|k} &\triangleq \mathbf{C}(\mathbf{z}_k)\mathbf{P}^x_{k+i|k}\mathbf{C}^\top(\mathbf{z}_k) + \mathbf{R}(\mathbf{z}_k) + \mathbf{L}_i\left[\mathbf{I}_{i+1}\otimes\left(\mathrm{diag}(\pi_{k|k}) - \pi_{k|k}\pi_{k|k}^\top\right)\right]\mathbf{L}_i^\top + \mathbf{D}(\mathbf{z}_k)\mathbf{\Gamma}(\mathbf{z}_k)\mathbf{D}^\top(\mathbf{z}_k) \\
&+ \mathbf{C}(\mathbf{z}_k)\left(\mathbf{P}^L_{qu} - \mathbf{A}^i(\mathbf{z}_k)\mathbf{P}^L_{qu}\left(\mathbf{A}^\top(\mathbf{z}_k)\right)^i\right)\mathbf{C}^\top(\mathbf{z}_k) \\
\mathbf{V}_{k+i,k+j|k} &\triangleq \mathbf{C}(\mathbf{z}_k)\mathbf{P}^x_{k+i,k+j|k}\mathbf{C}^\top(\mathbf{z}_k) + \mathbf{C}(\mathbf{z}_k)\left(\mathbf{P}^L_{qu} - \mathbf{A}^i(\mathbf{z}_k)\mathbf{P}^L_{qu}\left(\mathbf{A}^\top(\mathbf{z}_k)\right)^i\right)\left(\mathbf{A}^\top(\mathbf{z}_k)\right)^{j-i}\mathbf{C}^\top(\mathbf{z}_k) \\
&+ \mathbf{L}_i\left[\mathbf{1}_{i+1}\mathbf{1}^\top_{j+1}\otimes\left(\mathrm{diag}(\pi_{k|k}) - \pi_{k|k}\pi_{k|k}^\top\right)\right]\mathbf{L}_j^\top + \mathbf{D}(\mathbf{z}_k)\mathbf{\Gamma}(\mathbf{z}_k)\mathbf{B}^\top(\mathbf{z}_k)\left(\mathbf{A}^\top(\mathbf{z}_k)\right)^{j-i-1}\mathbf{C}^\top(\mathbf{z}_k) \\
\mathbf{P}^x_{k+i|k} &\approx \mathbf{A}(\mathbf{z}_k)^j(\hat{\mathbf{P}}^R_{xx} - \mathbf{P}^L_{xx})\left(\mathbf{A}^\top(\mathbf{z}_k)\right)^j + \mathbf{P}^L_{xx} \text{ (Recall Eqn.28)} \\
\mathbf{P}^x_{k+i,k+j|k} &\approx \mathbf{A}(\mathbf{z}_k)^i(\hat{\mathbf{P}}^R_{xx} - \mathbf{P}^L_{xx})\left(\mathbf{A}^\top(\mathbf{z}_k)\right)^j + \mathbf{P}^L_{xx}\left(\mathbf{A}^\top(\mathbf{z}_k)\right)^{j-i} \text{ (Recall Eqn.30)} \\
\text{where } \mathbf{Z}_{i+1} &= \mathbf{Z}_i\mathbf{G}^\top(\mathbf{z}_k) + \mathbf{C}(\mathbf{z}_k)\mathbf{A}^i(\mathbf{z}_k)\mathbf{B}(\mathbf{z}_k)\mathbf{H}(\mathbf{z}_k), \quad \mathbf{Z}_0 = \mathbf{D}(\mathbf{z}_k)\mathbf{H}(\mathbf{z}_k) \\
\text{and } \mathbf{L}_i &\triangleq \begin{bmatrix} \mathbf{G}^i(\mathbf{z}_k)\mathbf{H}^\top(\mathbf{z}_k)\mathbf{D}^\top(\mathbf{z}_k) \\ \mathbf{G}^{i-1}(\mathbf{z}_k)\mathbf{H}^\top(\mathbf{z}_k)\mathbf{B}^\top(\mathbf{z}_k)\mathbf{C}^\top(\mathbf{z}_k) \\ \vdots \\ \mathbf{G}\mathbf{H}^\top(\mathbf{z}_k)\mathbf{B}^\top(\mathbf{z}_k)\left(\mathbf{A}^\top(\mathbf{z}_k)\right)^{i-2}\mathbf{C}^\top(\mathbf{z}_k) \\ \mathbf{H}^\top(\mathbf{z}_k)\mathbf{B}^\top(\mathbf{z}_k)\left(\mathbf{A}^\top(\mathbf{z}_k)\right)^{i-1}\mathbf{C}^\top(\mathbf{z}_k) \end{bmatrix}^\top, \quad \text{Note } \mathbf{Z}_i = \mathbf{L}_i\left(\mathbf{1}_{i+1}\otimes\mathbf{I}_M\right)
\end{aligned}
$$

Fig. 11. Formulae for $\mu_{\mathbf{y}_d}$, $\Sigma_{\mathbf{y}_d}$, and $\hat{\Sigma}_{\mathbf{y}_d}$, Case #2